RSC Advances

PAPER

View Article Online
View Journal | View Issue

Cite this: *RSC Adv.*, 2021, **11**, 15

Self-reversible mechanofluorochromism of AIE-active C6-unsubstituted tetrahydropyrimidine derivatives†

Yanshan Liu, * Yunhui Liao, Ziwei Ye, Lina Chen, Yun He, Yifan Huang, Yingyu Lai, Junguo Chen and Qiuhua Zhu *

The mechanofluorochromic properties of three C6-unsubstituted tetrahydropyrimidines (THPs), namely, diethyl 1,2,3-triphenyl-1,2,3,6-tetrahydropyrimidine-4,5-dicarboxylate (**1**), dimethyl 1,2,3-tri(4-trifluoromethylphenyl)-1,2,3,6-tetrahydropyrimidine-4,5-dicarboxylate (**2**), and dimethyl 1,2,3-tri(3-trifluoromethylphenyl)-1,2,3,6-tetrahydropyrimidine-4,5-dicarboxylate (**3**), with aggregation-induced emission (AIE) characteristics were investigated. The blue-green/cyan emissions of the three THPs can be switched reversibly by a grinding–fuming/heating process, with the change in maximum emission wavelength (λ_{em}) up to 57 nm and the decrease of fluorescence quantum yields (Φ_F). Interestingly, the green or cyan fluorescence of the ground powder (λ_{em} is located at 481, 470 and 477 nm for **1b**, **2** and **3**, respectively) can spontaneously recover to the original blue (λ_{em} is located at 434, 442 and 436 nm for **1b**, **2** and **3**, respectively) in 1–2 d at room temperature without any external stimulation. X-ray single-crystal diffraction, powder X-ray diffraction (XRD) and differential scanning calorimetry (DSC) studies demonstrate that the conversion between the molecular packing modes is the main reason for the mechanofluorochromism and the spontaneously recoverable mechanofluorochromism relates to intermolecular hydrogen bonds. The sensitively and/or spontaneously recoverable mechanofluorochromism of these THPs is expected to have great potential in sensing, optical recording and self-healing fluorescent materials.

Received 29th October 2020
Accepted 4th December 2020

DOI: 10.1039/d0ra09209f

rsc.li/rsc-advances

1. Introduction

Organic mechanofluorochromic materials are a class of smart materials that exhibit color change upon external physical stimulus (such as pressure, vapor or heat) and have attracted intense attention because of their fundamental importance and potential applications in optical recording, optoelectronic devices, security papers, and sensors.[1–7] However, the mechanofluorochromic behavior of organic emissive materials is often difficult to observe because of the notorious aggregation-caused quenching (ACQ) effects in the condensed state, which would also limit the practical application of these materials.[8,9] In 2001, Tang *et al.* discovered a new phenomenon of aggregation-induced emission (AIE),[10] and proposed that the restriction of intramolecular motion is the main reason for the AIE effect,[11–13] and since then much effort has been devoted to designing and synthesizing propeller-shaped molecules to create solid state luminophores.[1,11–15] Interestingly, many AIE luminogens were also found to exhibit mechanofluorochromism.[5,16–19] In recent years, a number of mechanofluorochromic and AIE-active organic molecules, including tetraphenylethene-,[16,20–23] triphenylethene-,[24–26] difluoroboron complex-,[18,27–29] anthracene-,[30–32] cyanostilbene-[19,33,34] and triphenylamine-based[35–37] derivatives, have been investigated.[1,2] Changes in molecular conformation and packing modes have proven to be the main factors that influencing the switching and alternation of the emissions of the fluorophores.[20,25,32,38–42] However, the design and synthesis of new economic mechanofluorochromic organic compounds, and the in-depth understanding of the origin of mechanofluorochromism, still remains to be a challenge.[9,25,38,43] Comparing with the external-stimuli-controlled fluorescence switching, the self-recovery of the fluorescence of organic molecules has been seldom reported.[26,36,44,45] It will be interesting to have a research about this spontaneous recovery, which may have potential in self-healing materials.

In 2011, we have developed an economic and efficient five-component reaction (5CR) for the synthesis of a novel series of racemic AIE-active C6-unsubstituted tetrahydropyrimidine derivatives.[46] These THPs are non-luminescent in dilute solutions, but become highly emissive in the aggregate states.

Guangdong Provincial Key Laboratory of New Drug Screening, School of Pharmaceutical Sciences, Southern Medical University, Guangzhou, 510515, China. E-mail: liuys9@smu.edu.cn; zhuqh@smu.edu.cn

† Electronic supplementary information (ESI) available: Crystallographic data, ^{1}H NMR and ^{13}C NMR spectra, fluorescence decay profiles and other data of THPs **1–3**. CCDC 2020055 and 2020056. For ESI and crystallographic data in CIF or other electronic format see DOI: 10.1039/d0ra09209f

Different from other conventional AIE-active molecules, the solid-state luminescence of the THPs arises from the high conjugation formed by the through-space and through-bond electron coupling and the efficient enantiomeric packing modes in aggregates.[47,48] Our research has showed that the THPs could be used as sensitive thermometers in different temperature ranges,[49] fluorescent bioprobes for cell imaging,[50] and unique fluorescence-turn-on probes for the determination of the critical micelle concentration of ion surfactants.[51,52] Excitingly, we recently found that one of the THPs, dimethyl 1,3-bis(4-bromophenyl)-2-phenyl-1,2,3,6-tetrahydropyrimidine-4,5-dicarboxylate (Me-THP-2Br), exhibited highly sensitive and external-stimuli-controlled reversible fluorescence switching between purple and green upon grinding and fuming or heating.[38] The research about the three polymorphic crystals and amorphous state with distinctly different fluorescence of Me-THP-2Br indicated that the mechanofluorochromism correlates with conversion between the paired and unpaired packing modes of the *R*- and *S*-enantiomers (*RS*-paired and *RR*/*SS*-overlapped packing modes).[38] Considering the easy preparation and excellent AIE characteristics of the THPs, we further investigate the mechanofluorochromic behaviors of other compounds, and find that the fluorescence of almost all investigated THPs in ground powder can revert to their original fluorescence in crystals upon fuming or heating. And even more amazing, several THPs (**1–3** in Fig. 1) in ground powder can self-recover to their original fluorescence in crystals. In this paper, we investigated the self-reversible mechanofluorochromism in detail to further elucidate the mechanism of the self-reversible mechanofluorochromism of organic AIE compounds.

2. Experimental

2.1. Materials and measurements

Photos were taken by MEIZU MX4 under UV 365 nm. IR spectra were obtained as potassium bromide pellets with Nicolet iS50 spectrometer (Thermo Fisher). ^{1}H (400 MHz) and ^{13}C NMR (100.6 MHz) spectra were recorded on Bruker AVANCE III 400 spectrometer with $CDCl_3$ as the solvent. ^{1}H shifts were referenced to $CDCl_3$ at 7.26 ppm. ^{13}C shifts were referenced to $CDCl_3$ at 77 ppm. TLC was performed using commercially available 100–400 mesh silica gel plates (GF_{254}). UV-Vis spectra were measured on UV-5500PC (in solution) and U-3010 (in solid) spectrophotometer respectively. Fluorescence spectra were recorded by Shimadzu RF-5301PC spectrometer. The absolute fluorescence quantum yields and fluorescence lifetimes were measured on Edinburgh FLS 980 fluorescence spectrophotometer. XRD patterns were recorded at room temperature with an X'Pert Pro diffractometer operated at 40 kV voltage and 40 mA current with Cu Kα irradiation at λ = 1.5418 Å. DSC measurements were recorded on a NETZSCH thermal analyzer (NETZSCH 214 or DSC 200 F3) at heating and cooling rates of 10 K min^{-1} under an N_2 atmosphere. The X-ray single-crystal diffraction data were measured by Bruker D8 Venture. HOMO and LUMO were calculated by Gaussian 09 program. The ground powders were prepared by grinding the as-prepared crystals with a pestle in the mortar. The fumed samples were obtained by fuming the ground powder with dichloromethane (DCM) vapor.

Unless otherwise stated, all reagents and solvents were purchased from commercial suppliers and used without further purification.

2.2. Preparation of THPs 1–3

THPs **1–3** were synthesized by adopting the 5CR that we developed.[46] The characterization data of **1** and **3** are the same as those reported in our previous work,[46,53] and those for **2** see the ESI.† The polymorphic crystals of 1 and the crystals of 2 and 3 were prepared by recrystallization from DCM/*n*-hexane solution.

3. Results and discussion

3.1. Optical properties of THPs 1–3 in solutions and solid-states

The chemical structures and photos taken under 365 nm UV light of the as-prepared crystals of THPs **1–3** are shown in Fig. 1.

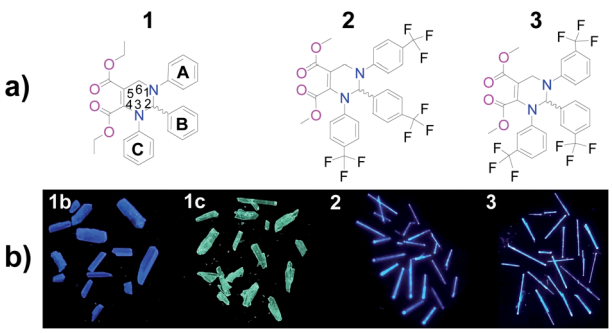

Fig. 1 (a) Chemical structures of THPs **1–3** and (b) photos of their as-prepared crystals (under 365 nm UV light). **1b**: blue crystals of **1**; **1c**: cyan crystals of **1**.

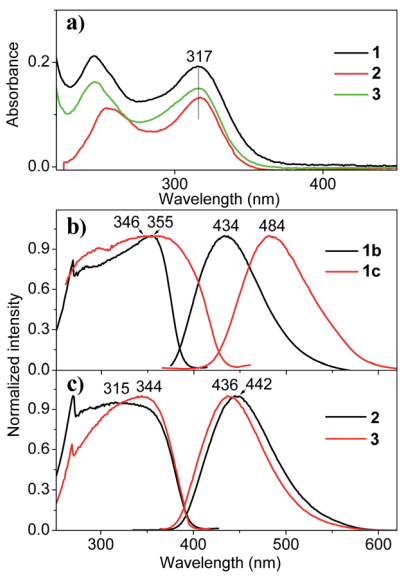

Fig. 2 Optical properties of THPs **1–3**. (a) Absorption spectra of THPs **1–3** in cyclohexane solutions (1.0×10^{-5} M). (b) and (c) Excitation (left) and emission (right) (excited at emission peak marked in the left excitation spectra) spectra of **1b**, **1c**, **2** and **3**, respectively.

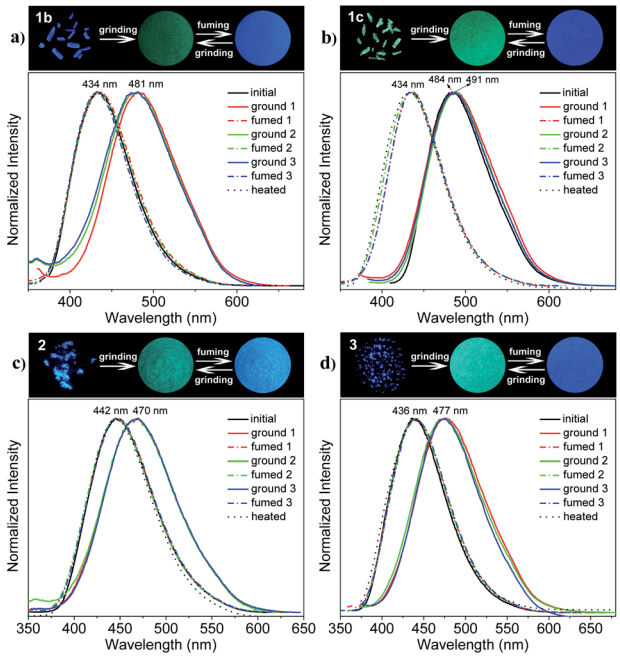

Fig. 3 Reversible grinding–fuming-controlled fluorescence-color switching of THPs **1–3** respectively. Photos of the initial crystals (left), ground powders (middle) and fumed samples (right) taken under 365 nm light (upper) and their emission spectra (lower) in three grinding–fuming cycles of **1b** (a), **1c** (b), **2** (c) and **3** (d), respectively.

The absorption spectra of THPs **1–3** in cyclohexane in Fig. 2a show a peak at 317 nm, corresponding to an n–π* transition. The three THPs are non-emissive in solutions, however, they emit brightly in solid states, with Φ_F (excited at 350 nm) equals to 72.0, 93.0, 96.0 and 97.0% for **1b**, **1c**, **2** and **3**, respectively, which means that they are highly AIE-active. The excitation and emission spectra of THPs **1**, **2** and **3** are displayed in Fig. 2b and c respectively.

3.2. Mechanofluorochromic characteristics of THPs 1–3

The mechanofluorochromic properties of the polymorphic crystals of THP **1** were investigated through the grinding–fuming/heating process firstly. As shown in Fig. 3a and b (upper), the as-synthesized **1b** and **1c** crystals emit intense blue and cyan light under UV irradiation, with λ_{em} equals to 434 and 484 nm respectively. They change into green-emitting powders with λ_{em} locates at 481 and 491 nm respectively, after grinding, showing an obvious mechanofluorochromic effect. Furthermore, the ground powder of **1b** could revert back quickly to blue-emitting solid similar to the original **1b** crystal, with λ_{em} = 434 nm, after fuming with DCM vapor for 2 min or heated under 110 °C for 20 min. But it took more than 1 h of fuming or heating for the ground powder of **1c** to recover back to blue-emitting crystal with λ_{em} = 434 nm. The blue-green emission could be switched repeatedly by grinding and fuming or heating for many times. The emission spectra of **1b** and **1c** in the as-synthesized crystals (black solid line), ground powders (solid color lines) and fumed or heated states (dotted color or black lines) in three grinding–fuming cycles are shown in Fig. 3a and b (lower).

Then, the mechanofluorochromic behaviors of THPs **2** and **3** were investigated. As shown in Fig. 3c and d (upper), the as-synthesized **2** and **3** solids emit blue light with λ_{em} equal to 442 and 436 nm under UV irradiation, and their emitting colors turn into cyan with λ_{em} locates at 470 and 477 nm, respectively, after grinding. In addition, the cyan-emitting ground powders of **2** and **3** could be transferred into blue-emitting solids similar to the as-synthesized crystals after fuming with DCM for 2 min or heated under 110 °C for 20 min. This blue-cyan emission could also be converted back and forth by grinding and fuming or heating for many times. Fig. 3c and d (lower) show the emission spectra of **2** and **3** in the as-synthesized crystals (black solid line), ground powders (solid color lines) and fumed or heated states (dotted color or black lines) in three grinding–fuming cycles. Furthermore, the Φ_F (excited at 380 nm) of the ground powders of **1b**, **1c**, **2** and **3** are lower (16.0, 55.0, 51.1 and 61.4%, respectively) than those of their original crystals (72.0, 93.0, 96.0 and 97.0%, respectively). It means that grinding can not only switch the emission color but also change the luminescence efficiency of the THPs. The fluorescent lifetimes (τ, excited at 360 nm) of **1b**, **1c**, **2** and **3** are 7.1, 14.4, 10.1 and 8.3 ns, respectively, and those of the corresponding ground powders of **1b**, **1c**, **2** and **3** are 5.7, 9.9, 6.3 and 7.1 ns, respectively. The radiative rate constant (k_r) and non-radiative rate constant (k_{nr}) of THPs **1–3** in crystals and ground powders were calculated (Table 1) according to the Φ_F and τ values, that is, $k_r = \Phi_F/\tau$ and $k_{nr} = (1 - \Phi_F)/\tau$. It can be seen that the k_r values of the crystals are in the range of 0.65–1.17 × 10^8 s^{-1}, and those of the ground powders are in the range of 0.28–0.86 × 10^8 s^{-1}. The k_{nr} values of the crystals are in the range of 0.04–0.39 × 10^8 s^{-1}, while those of the ground powders are in the range of 0.45–1.47 × 10^8 s^{-1}. After grinding, the k_r values change slightly except **1b**, which means that the changes in molecular conformation and/or packing mode are slightly except **1b**. Whereas the k_{nr} values of ground powders are much smaller than those of crystals

Table 1 Optical properties of the initial crystals, ground powders, fumed and heated states of THPs **1–3**

	λ_{em}/nm					Φ_F (%)		τ/ns		$k_r/s^{-1} \times 10^{-8}$		$k_{nr}/s^{-1} \times 10^{-8}$	
THPs	Initial	Ground	Fumed	Heated	$\Delta\lambda_{em}$/nm	Initial	Ground	Initial	Ground	Initial	Ground	Initial	Ground
1b	434	481	434	434	47	72.0	16.0	7.1	5.7	1.01	0.28	0.39	1.47
1c	484	491	434	434	57	93.0	55.0	14.4	9.9	0.65	0.56	0.05	0.45
2	442	470	442	442	28	96.0	51.1	10.1	6.3	0.95	0.81	0.04	0.78
3	436	477	436	436	31	97.0	61.4	8.3	7.1	1.17	0.86	0.04	0.54

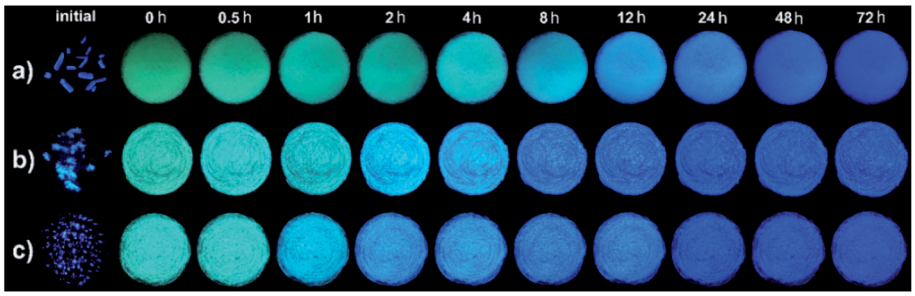

Fig. 4 Photos of the initial crystals and ground samples kept for different time of **1b** (a), **2** (b) and **3** (c) taken under 365 nm light respectively.

because of the restriction of intramolecular motion (RIM), thus leading to the decrease of the fluorescence. These phenomena indicate that the racemic AIE-active tetrahydropyrimidine derivatives possess sensitive and reversible mechanofluorochromism with the change of λ_{em} up to 57 nm. The optical properties of the initial crystals, ground powders, fumed and heated states of THPs **1–3** are summarized in Table 1. The photos of the as-synthesized **1b**, **1c**, **2** and **3** and their corresponding ground powder under natural light are shown in Fig. S1,† and the absorption spectra of the different solid states of **1b**, **1c**, **2** and **3** are shown in Fig. S2.† The fluorescence decay profiles are displayed in Fig. S3.† The fluorescent lifetimes of **1b** and **1c** were reported previously,[47] and those of the others were measured in this work.

3.3. Self-reversible mechanofluorochromic characteristics of THPs 1–3

During the above process of mechanofluorochromism investigation, we found that the emitting colors of THPs **1b**, **2** and **3** in green ground power could spontaneously recover to blue under room temperature without the exertion of any external stimulation. So we carefully observed and systematically studied the self-reversible characteristics of THPs **1–3**. As shown in Fig. 4, the green or cyan-emitting ground powders of **1b**, **2** and **3** can all self-recover to blue-emitting solids in 1–2 d under 30 °C, exhibiting wonderful spontaneous fluorescence recovery. But for **1c**, the ground powder didn't show fluorescence change when stood still.

3.4. Mechanism of the reversible mechanofluorochromism of THPs 1–3

To get insight into the mechanism of the reversible mechanofluorochromic characteristics, the XRD analysis was conducted on the three THPs. As demonstrated in Fig. 5a and c, the as-synthesized crystals of THPs **1–3** (**1–3**-initial) exhibit sharp and strong reflection peaks, suggesting highly ordered and different molecular arrangements of the crystals. There are only very weak or no reflection peaks for the corresponding ground powders of THPs **1–3**, indicating amorphous states with short-range ordered molecular arrangements after grinding. The diffraction patterns of the fumed states of the ground powder of **1b** (**1b**-fumed) and **1c** (**1c**-fumed) samples are almost identical to the as-synthesized **1b**, and those of the **2**-fumed and **3**-fumed samples are almost identical to the as-synthesized **2** and **3** solids respectively. These results show that the ground powders of the THPs can all revert back to their original blue-emitting crystals by fuming, which demonstrates that the as-synthesized crystals are more stable solid states.

DSC measurements were also conducted on the samples to investigate the phase transition during the mechanofluorochromic process. As shown in Fig. 5b and d, there are no transition peaks before melting points in the heating curves of the as-synthesized **1b**, **1c**, **2** and **3** crystals. However, it is found that the ground powders of **1b**, **2** and **3** exhibit clear exothermic peaks at around 55.4, 82.3 and 57.6 °C in the DSC curves, respectively, corresponding to the cold-crystallization transitions. These results mean that the ground powders of these samples are in metastable phases, and they transform into more stable crystalline phases *via* an exothermal recrystallization process. But for the ground powder of **1c**, there is no clear cold-crystallization peak is observed, instead, there appears another endothermic peak at approximately 114.2 °C before its melting point (126.8 °C) in the heating curve, which is different

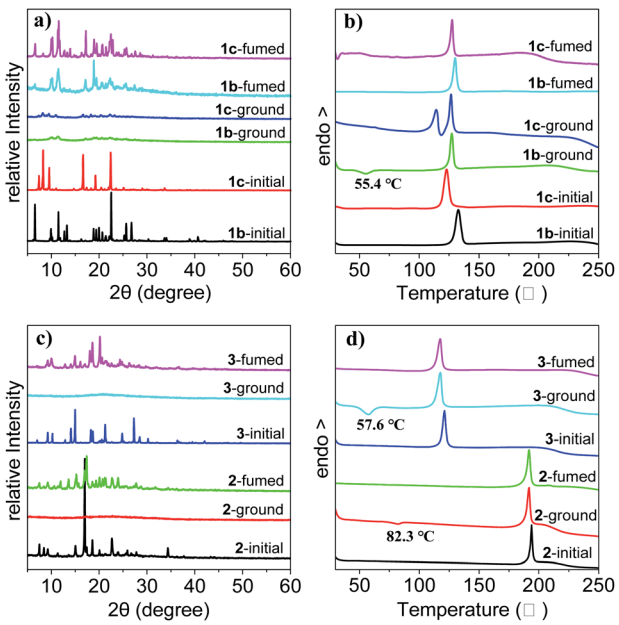

Fig. 5 XRD patterns of **1b** and **1c** (a), **2** and **3** (c) and DSC curves of **1b** and **1c** (b), **2** and **3** (d) in initial, ground and fumed states, respectively.

from the ground powders of other crystals. During the mechanofluorochromic process, we found that **1c** was much less responsive to external stimuli than others, and it took much more time for it to transform into green-emitting powder by grinding or change into blue-emitting crystals by fuming. As we have reported in reference,[46] the **1c** crystals are the kinetically favored form of THP **1** which can be obtained from solutions at lower temperature or higher concentration, while the **1b** crystals are the thermodynamically favored form which can be obtained from solutions at higher temperature or lower concentration. During the heating process, the **1c**-ground powders first recrystallized partly into kinetically favored **1c** crystals at relatively lower temperature, and they might melt with the increasing of temperature and transform into thermodynamically favored **1b** crystals, thus leading to the appearance of another endothermic melting peak at 114.2 °C in the DSC curve of the **1c**-ground powders. Based on these XRD and DSC results, we can consider that the transformation between the amorphous and crystalline states is responsible for the reversible mechanofluorochromic behaviors of these THPs.

To better understand the reversible mechanofluorochromic behaviors of these THPs, it is necessary to get single crystals. Fortunately, the quality single crystals of THPs **2** and **3** with emission wavelengths 442 and 436 nm, respectively, were obtained in this work, and the polymorphic single crystals **1b** and **1c** of THP **1** were obtained as we reported previously.[46] The crystallographic data of THPs **2** and **3** are listed in Table S1,† it shows that the space groups of **2** and **3** are *Pbca* and $P12_1/n1$, respectively. To better understand their electronic structures, the HOMOs and LUMOs of **2** and **3** were obtained by DFT/B3LYP/6-31G Gaussian calculations based on the molecular conformations in single crystal. The HOMO and LUMO plots are given in Fig. 6. Their HOMOs, LUMOs and through-space conjugations (the area marked in color circles) are similar as those reported in our previous work.[47,53] Molecular simulation of THPs **1–3** using DFT/B3LYP/6-31G method was also done and the optimized geometric structures and electron density plots of HOMOs and LUMOs are given in Fig. S4,† and the comparison of the HOMO, LUMO, energy gap and Gibbs free energy of THPs **1–3** in single crystal and optimized geometry by simulation is shown in Table 2. The Gibbs free energies of the conformations in crystals are about 200–300 kcal mol^{-1} higher than that in their optimized geometries, which suggests that the molecules of THPs **1–3** in crystals exist in the form of non-optimized geometry due to the molecular interactions. **1b** is formed under thermodynamically condition, while **1c** is formed under kinetically condition. This means the stability of **1b** is better than that of **1c** crystal, that is, the energy of the former is lower than the latter. However, the energy of the molecular conformation in **1b** is a little higher than that in **1c** crystal, showing that the decrease of the energy of **1b** comes from molecular interactions. These also demonstrate that the self-recover energy mainly originates from molecular interactions. Fig. 7 presents the molecular packing modes, intermolecular interactions and conformations of **2** and **3**, respectively, and the intra- and intermolecular short-ring interactions and hydrogen bonds in THPs **1–3** are summarized in Table S2.†

Fig. 7 shows that both blue-emitting THPs **2** and **3** crystals adopt the unpaired *R*- and *R*-enantiomer or *S*- and *S*-enantiomer packing mode (*RR*/*SS*-overlapped). Our previous investigation[47,53] has demonstrated that the blue-emitting **1b** polymorph adopted the paired *R*- and *S*-enantiomer packing mode (*RS*-paired) with short-range ring interactions only existing between paired *R*- and *S*-enantiomers, while the cyan-emitting **1c** polymorph adopted the *RR*/*SS*-overlapped packing mode with short-range ring interactions existing among all zigzag-aligned *R*- or *S*-enantiomers. The *RR*/*SS*-packed and *R*/*S*-packed crystals of THPs **1** are formed in kinetically and thermodynamically conditions, respectively.[46,47,53] According to these results, together with our previous study, it can be concluded that the reversible mechanofluorochromic behaviors of THPs **1** originate from the conversion of metastable *RR*/*SS*-overlapped and stable *RS*-paired packing modes, similar as the reversible mechanofluorochromic behaviors of Me-THP-2Br that we reported previously.[38] We have prepared a series of polymorphs of THPs with different R^1–R^4 in single crystals, and studied the influence of molecular packing modes on their fluorescence properties.[47,53] The research results (see Table S3†) show that the polymorphs with shorter or shortest wavelength emission adopt *RS*-packing, while polymorphs with longer wavelength

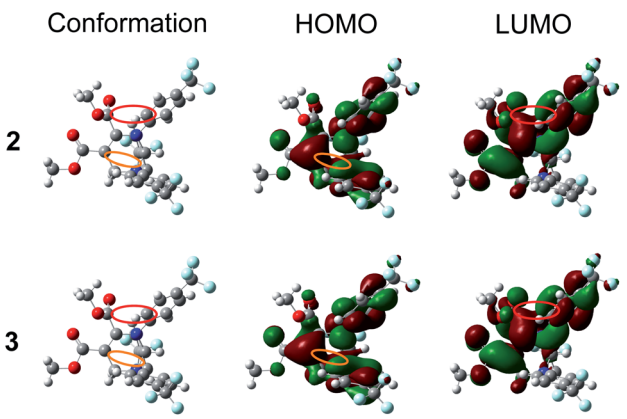

Fig. 6 Molecular conformations, HOMOs and LUMOs of **2** and **3** in single crystals.

Table 2 Comparison of the HOMO, LUMO, energy gap and Gibbs free energy of THPs **1–3** in single crystal and optimized geometry by simulation

THPs	Conformation	HOMO	LUMO	ΔE^a/eV	ΔG^b/kcal mol^{-1}
1	**1b**	−5.31	−0.94	4.47	−937031
	1c	−5.31	−1.16	4.15	−937037
	1opt^c	−5.31	−0.79	4.52	−937375
2	**2cry**^{d}	−6.33	−2.02	4.31	−1522350
	2opt	−5.94	−1.70	4.24	−1522549
3	**3cry**	−6.22	−1.89	4.33	−1522342
	3opt	−5.84	−1.53	4.31	−1522548

^{a} Band gap between the HOMO and LUMO. ^{b} Gibbs free energy. ^{c} Optimized geometry by simulation. ^{d} Single crystal.

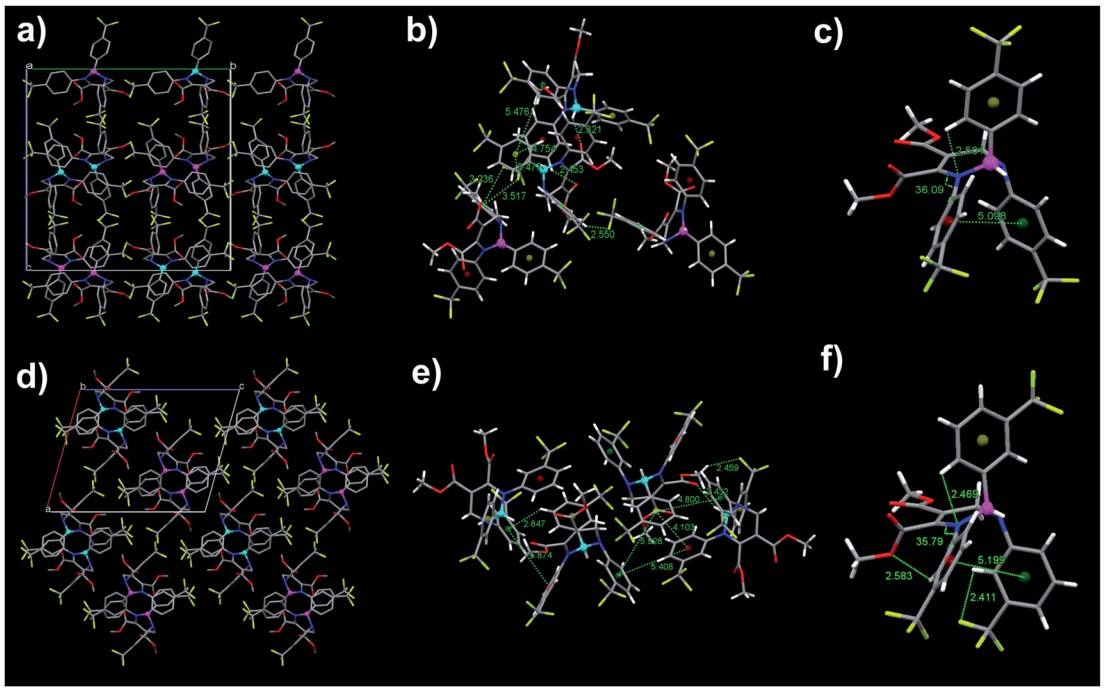

Fig. 7 The molecular packing modes, intermolecular interactions, and conformations (from left to right) of **2** (a–c) and **3** (d–f) in single crystals with emission wavelengths 442 (**2**) and 436 nm (**3**). Cyan and purples balls, respectively, represent the *R*- and *S*-configurations of chiral carbon. CCDC 2020055 and 2020056 for **2** and **3**, respectively.

emission adopt *RR*/*SS*-packing modes. For example, the λ_{em} value of **1b** with *RS*-packing mode is shorter than that of its polymorph **1c** with *RR*/*SS*-packing mode, and the λ_{em} value of **5p** with *RS*-packing mode is the shortest among three polymorphs (other two polymorphs are **5b** and **5c** with *RR*/*SS*-packing mode (see Table S3†)). From these, we can deduce that the ground **2** and **3** with longer λ_{em} values (470 and 477 nm) than those of their crystals (442 and 436 nm) with *RR*/*SS*-packing mode should possess *RR*/*SS*-packing mode. This means that the reversible mechanofluorochromism of THPs **2** and **3** originates from the conversion between two kinds of *RR*/*SS*-packing modes. The as-prepared crystals packed in *RS*-paired and *RR*/*SS*-overlapped packing modes are stable until they are melted because the tightly packed molecules can't move freely and undergo packing rearrangement. However, the ordered *RS*- or *RR*/*SS*-arrangements in the as-prepared solid states of THPs **1–3** are mostly destroyed upon grinding and hence the kinetically favored *RR*/*SS*-packing alignments with more planarized molecular conformations are formed, accompanied by a red shift in emission wavelengths, which can convert into thermodynamically stable *RS*-paired (THP **1**) or *RR*/*SS*-overlapped (THPs **2** and **3**) packing mode with short emission wavelength upon fuming or heating (for the schematical mechanism of the mechanofluorochromism of THPs, see our previous work[38]).

Zhang *et al.* had studied the mechanofluorochromic behaviors of three phenothiazine modified triphenylacrylonitrile derivatives, and proposed that the more twisted conformation is the reason for the fluorescence self-recovery of compound P10TPAN.[26] However, our experimental results do not support this conclusion. This is because that the purple-emitting polymorph of Me-THP-2Br (PC) with more twisted conformation (the dihedral angle value is 53.04°) than that of **1b** (the dihedral angle value is 49.24°) doesn't have self-reversible mechanofluorochromic characteristics. After carefully analyzing and comparing the molecular interactions in single crystals of **1b**, **2** and **3** with Me-THP-2Br in PC, we deduce that the self-reversible mechanofluorochromic characteristics of **1b**, **2** and **3** relates to intermolecular hydrogen bonds. There exist eight intermolecular hydrogen bonds in **1b** (6 × C–H···π, 2.930 Å; 2.837 Å; 2.971 Å; 2 × C–H···O, 2.487 Å), six intermolecular hydrogen bonds in **2** (2 × C–H···O, 2.453 Å; 2.321 Å; C–H···F, 2.550 Å; 3 × C–F···π, 3.236 Å; 3.517 Å; 3.477 Å), and three intermolecular hydrogen bonds in **3** (C–H···π, 2.847 Å; C–H···O, 2.432 Å; C–H···F, 2.459 Å), respectively (see Table S2†), while none exist in PC,[47] which means that the intermolecular hydrogen bond interaction in **1b**, **2** and **3** is much stronger than that in PC. During the grinding process, the stronger intermolecular interaction makes the molecular packing in **1b**, **2** and **3** more difficult to be destroyed, and the molecular packing can be easily restored along with the release of grinding. The DSC curve (Fig. 5b) shows that the cold-crystallization temperatures of **1b**, **2** and **3** are 55.4, 82.3 and 57.6 °C, respectively, which proves that the ground powder can recrystallize easily, meaning that the ground powders of THP **1b**, **2** and **3** packed in metastable *RR*/*SS*-mode can spontaneously change into stable blue-emitting *RS*- or *RR*/*SS*-packing mode owing to the relatively stronger hydrogen bond interactions in blue-emitting crystals. Since there is no such relatively stronger hydrogen bond in *RS*-paired mode, the ground powder of Me-THP-2Br packed in *RR*/*SS*-overlapped mode can't spontaneously change into stable *RS*-

paired mode. The self-reversible mechanofluorochromic behavior of these THPs may afford a new kind of smart self-healing fluorescence materials and have great potential in practical applications.

4. Conclusions

In summary, we have studied the reversible mechanofluorochromism of three racemic C6-unsubstituted tetrahydropyrimidine derivatives (THPs **1–3**) with AIE characteristics. The three THPs exhibit sensitive and reversible mechanofluorochromic behaviors, the blue-green/cyan emissions can be switched reversibly by grinding and fuming or heating. Furthermore, the ground powders of **1b**, **2** and **3** display fluorescence self-recovery without exertion of any external stimuli under room temperature. On the basis of photophysical, XRD, DSC, X-ray single-crystal diffraction results, we suggest that the reversible mechanofluorochromism of THPs originate from the conversion between the metastable *RR*/*SS*-packing and stable *RS*- or *RR*/*SS*-packing modes of enantiomers. Furthermore, we propose that the intermolecular hydrogen bond interaction may account for the fluorescence self-recovery of **1b**, **2** and **3** at room temperature. After grinding, the ordered *RS*- or *RR*/*SS*-packing can be converted into short-range ordered *RR*/*SS*-packing. Upon fuming or heating, the metastable amorphous state transforms into thermodynamically stable packing modes, or self-recovers to its stable initial crystalline state without external stimuli at room temperature. The self-reversible mechanofluorochromic behavior of these THPs may afford a new kind of smart self-healing fluorescence materials and have great potential in practical applications.

Conflicts of interest

There are no conflicts of interest to declare.

Acknowledgements

This work was supported by the Special Funds for the Cultivation of Guangdong College Students' Scientific and Technological Innovation ("Climbing Program" Special Funds) (pdjh2016a0092), and Guangdong Natural Science Foundation (2018A030313976).

Notes and references

1 J. Zhao, Z. Chi, Y. Zhang, Z. Mao, Z. Yang, E. Ubba and Z. Chi, *J. Mater. Chem. C*, 2018, **6**, 6327–6353.
2 X. Huang, L. Qian, Y. Zhou, M. Liu, Y. Cheng and H. Wu, *J. Mater. Chem. C*, 2018, **6**, 5075–5096.
3 P. Xue, J. Ding, P. Wang and R. Lu, *J. Mater. Chem. C*, 2016, **4**, 6688–6706.
4 Y. Sagara, S. Yamane, M. Mitani, C. Weder and T. Kato, *Adv. Mater.*, 2016, **28**, 1073–1095.
5 Z. Chi, X. Zhang, B. Xu, X. Zhou, C. Ma, Y. Zhang, S. Liu and J. Xu, *Chem. Soc. Rev.*, 2012, **41**, 3878–3896.
6 Y. Sagara and T. Kato, *Nat. Chem.*, 2009, **1**, 605–610.
7 T. Mutai, H. Satou and K. Araki, *Nat. Mater.*, 2005, **4**, 685–687.
8 R. Hu, N. L. C. Leung and B. Z. Tang, *Chem. Soc. Rev.*, 2014, **43**, 4494–4562.
9 W. Yuan, Y. Tan, Y. Gong, P. Lu, J. Lam, X. Shen, C. Feng, H. Sung, Y. Lu, I. D. Williams, J. Sun, Y. Zhang and B. Z. Tang, *Adv. Mater.*, 2013, **25**, 2837–2843.
10 J. Luo, Z. Xie, J. W. Lam, L. Cheng, H. Chen, C. Qiu, H. S. Kwok, X. Zhan, Y. Liu, D. Zhu and B. Z. Tang, *Chem. Commun.*, 2001, 1740–1741.
11 J. Mei, Y. Hong, J. W. Y. Lam, A. Qin, Y. Tang and B. Z. Tang, *Adv. Mater.*, 2014, **26**, 5429–5479.
12 Y. Hong, J. W. Lam and B. Z. Tang, *Chem. Soc. Rev.*, 2011, **40**, 5361–5388.
13 Y. Hong, J. W. Lam and B. Z. Tang, *Chem. Commun.*, 2009, 4332–4353.
14 G. Feng, R. T. K. Kwok, B. Z. Tang and B. Liu, *Appl. Phys. Rev.*, 2017, **4**, 021307.
15 H. Wang, E. G. Zhao, J. W. Y. Lam and B. Z. Tang, *Mater. Today*, 2015, **18**, 365–377.
16 X. Zhang, Z. Chi, H. Li, B. Xu, X. Li, W. Zhou, S. Liu, Y. Zhang and J. Xu, *Chem.–Asian J.*, 2011, **6**, 808–811.
17 H. Li, X. Zhang, Z. Chi, B. Xu, W. Zhou, S. Liu, Y. Zhang and J. Xu, *Org. Lett.*, 2011, **13**, 556–559.
18 G. Zhang, J. Lu, M. Sabat and C. L. Fraser, *J. Am. Chem. Soc.*, 2010, **132**, 2160–2162.
19 S. J. Yoon, J. W. Chung, J. Gierschner, K. S. Kim, M. G. Choi, D. Kim and S. Y. Park, *J. Am. Chem. Soc.*, 2010, **132**, 13675–13683.
20 J. Wang, J. Mei, R. Hu, J. Z. Sun, A. Qin and B. Z. Tang, *J. Am. Chem. Soc.*, 2012, **134**, 9956–9966.
21 H. Gao, D. Xu, X. Liu, A. Han, L. Zhou, C. Zhang, Z. Li and J. Dang, *Dyes Pigm.*, 2017, **139**, 157–165.
22 M. Chen, L. Li, H. Nie, J. Tong, L. Yan, B. Xu, J. Z. Sun, W. Tian, Z. Zhao, A. Qin and B. Z. Tang, *Chem. Sci.*, 2015, **6**, 1932–1937.
23 J. Tong, Y. Wang, J. Mei, J. Wang, A. Qin, J. Z. Sun and B. Z. Tang, *Chem.–Eur. J.*, 2014, **20**, 4661–4670.
24 Z. Yang, Z. Chi, T. Yu, X. Zhang, M. Chen, B. Xu, S. Liu, Y. Zhang and J. Xu, *J. Mater. Chem. C*, 2009, **19**, 5541–5546.
25 Y. Zhang, Q. Song, K. Wang, W. Mao, F. Cao, J. Sun, L. Zhan, Y. Lv, Y. Ma and B. Zou, *J. Mater. Chem. C*, 2015, **3**, 3049–3054.
26 G. Zhang, J. Sun, P. Xue, Z. Zhang, P. Gong, J. Peng and R. Lu, *J. Mater. Chem. C*, 2015, **3**, 2925–2932.
27 P. Galer, R. C. Korosec, M. Vidmar and B. Sket, *J. Am. Chem. Soc.*, 2014, **136**, 7383–7394.
28 Z. Zhang, Z. Wu, J. Sun, B. Yao and R. Lu, *J. Mater. Chem. C*, 2016, **4**, 2854–2861.
29 M. Liu, L. Zhai, J. Sun, P. Xue, P. Gong, Z. Zhang, J. Sun and R. Lu, *Dyes Pigm.*, 2016, **128**, 271–278.
30 X. Zhang, Z. Chi, X. Zhou, S. Liu, Y. Zhang and J. Xu, *J. Phys. Chem. C*, 2012, **116**, 23629–23638.
31 X. Zhang, Z. Ma, Y. Yang, X. Zhang, Z. Chi, S. Liu, J. Xu, X. Jia and Y. Wei, *Tetrahedron*, 2014, **70**, 924–929.

32 Y. Dong, B. Xu, J. Zhang, X. Tan, L. Wang, J. Chen, H. Lv, S. Wen, B. Li and L. Ye, *Angew. Chem., Int. Ed.*, 2012, **51**, 10782–10785.
33 H. Zhao, Y. Wang, S. Harrington, L. Ma, S. Hu, X. Wu, H. Tang, M. Xue and Y. Wang, *RSC Adv.*, 2016, **6**, 66477–66483.
34 S. J. Yoon and S. Park, *J. Mater. Chem.*, 2011, **21**, 8338–8346.
35 M. Chen, H. Nie, B. Song, L. Li, J. Sun, A. Qin and B. Z. Tang, *J. Mater. Chem. C*, 2016, **4**, 2901–2908.
36 P. Hariharan, N. Venkataramanan, D. Moon and S. Anthony, *J. Phys. Chem. C*, 2015, **119**, 9460–9469.
37 P. Xue, P. Chen, J. Jia, Q. Xu, J. Sun, B. Yao, Z. Zhang and R. Lu, *Chem. Commun.*, 2014, **50**, 2569–2571.
38 Y. Liu, Z. Ye, M. Zhao, Q. Chen, Y. Wang and Q. Zhu, *Dyes Pigm.*, 2017, **145**, 391–398.
39 Y. Ji, Z. Peng, B. Tong, J. Shi, J. Zhi and Y. Dong, *Dyes Pigm.*, 2017, **139**, 664–671.
40 Z. He, L. Zhang, J. Mei, T. Zhang, J. W. Y. Lam, Z. Shuai, Y. Q. Dong and B. Z. Tang, *Chem. Mater.*, 2015, **27**, 6601–6607.
41 M. Yuan, D. Wang, P. Xue, W. Wang, J. Wang, Q. Tu, Z. Liu, Y. Liu, Y. Zhang and J. Wang, *Chem. Mater.*, 2014, **26**, 2467–2477.
42 R. Li, S. Xiao, Y. Li, Q. Lin, R. Zhang, J. Zhao, C. Yang, K. Zou, D. Li and T. Yi, *Chem. Sci.*, 2014, **5**, 3922–3928.
43 Y. Lai, J. Huang, S. Wu, Q. Zhu and Y. Liu, *Dyes Pigm.*, 2019, **166**, 8–14.
44 X. Luo, W. Zhao, J. Shi, C. Li, Z. Liu, Z. Bo, Y. Q. Dong and B. Z. Tang, *J. Phys. Chem. C*, 2012, **116**, 21967–21972.
45 X. Luo, J. Li, C. Li, L. Heng, Y. Q. Dong, Z. Liu, Z. Bo and B. Z. Tang, *Adv. Mater.*, 2011, **23**, 3261–3265.
46 Q. Zhu, L. Huang, Z. Chen, S. Zheng, L. Lv, Z. Zhu, D. Cao, H. Jiang and S. Liu, *Chem.–Eur. J.*, 2013, **19**, 1268–1280.
47 Q. Zhu, Y. Zhang, H. Nie, Z. Zhao, S. Liu, K. S. Wong and B. Z. Tang, *Chem. Sci.*, 2015, **6**, 4690–4697.
48 Q. Zhu, C. Dai, C. Huang, S. Zheng and Y. Tian, *J. Phys. Chem. C*, 2017, **121**, 25503–25508.
49 Q. Zhu, W. Yang, S. Zheng, H. H. Y. Sung, I. D. Williams, S. Liu and B. Z. Tang, *J. Mater. Chem. C*, 2016, **4**, 7383–7386.
50 S. Zheng, C. Huang, X. Zhao, Y. Zhang, S. Liu and Q. Zhu, *Spectrochim. Acta, Part A*, 2018, **189**, 231–238.
51 X. Cai, W. Yang, L. Huang, Q. Zhu and S. Liu, *Sens. Actuators, B*, 2015, **219**, 251–260.
52 Q. Zhu, L. Huang, J. Su and S. Liu, *Chem. Commun.*, 2014, **50**, 1107–1109.
53 Q. Zhu, S. Wu, S. Zheng, Z. Ye, C. Huang and Y. Liu, *Dyes Pigm.*, 2019, **162**, 543–551.